Journal of Fluorine Chemistry 129 (2008) 1187–1192

Contents lists available at ScienceDirect

Journal of Fluorine Chemistry

journal homepage: www.elsevier.com/locate/fluor

Molecular structure and IR absorption spectra of perfluorinated aldehyde hydrates (n-$C_xF_{2x+1}CH(OH)_2$, x = 1–4)

N. Kanno [a,1], K. Tonokura [a,*], M.D. Hurley [b], T.J. Wallington [b,**]

[a] Environmental Science Center, The University of Tokyo, 7-3-1 Hongo, Bunkyo-ku, Tokyo 113-0033, Japan
[b] Ford Motor Company, Mail Drop RIC-2122, Dearborn, MI 48121-2053, USA

ARTICLE INFO

Article history:
Received 5 August 2008
Received in revised form 16 September 2008
Accepted 16 September 2008
Available online 24 September 2008

Keywords:
Perfluorinated aldehyde hydrates
IR absorption
Molecular structure

ABSTRACT

Structures and IR absorption spectra of the conformational isomers of perfluorinated aldehyde hydrates, n-$C_xF_{2x+1}CH(OH)_2$, (x = 1–4) have been calculated using density functional theory (DFT) and compared to experimental FT-IR measurements. Two absorption peaks around 3600–3700 cm^{-1} were observed and are assigned to O–H stretching modes of OH groups with, and without, intramolecular hydrogen bonding. For n-$C_3F_7CH(OH)_2$, two absorption bands around 900–1000 cm^{-1} were observed in the experimental spectra, whereas only a single in-phase stretching mode of the (CF_3)–($C_2F_4CH(OH)_2$) and (C_3F_7)–($CH(OH)_2$) bonds was calculated for each conformer. The experimental spectra were well described by composite spectra of the thermal equilibrium mixture of different conformational isomers of n-$C_xF_{2x+1}CH(OH)_2$ calculated by DFT.

1. Introduction

Long-chain perfluoroalkyl carboxylic acids (PFCAs, $C_xF_{2x+1}COOH$, where x = 6–12) have been observed in fish [1,2] and mammals [3] in a range of locations around the world. PFCAs are not generally used directly in consumer or industrial materials, other than in aqueous film forming foams or as polymerization aids in fluoropolymer manufacture [4]. Thermolysis of fluoropolymers produces PFCAs, however the magnitude of this source appears insufficient to account for the observed global environmental burden of these compounds [5]. Three long range PFCA transport mechanisms have been discussed in the literature. Long range transport of PFCAs via ocean currents is possible [6]. An atmospheric transport route where polyfluorinated precursors are transported over long distances and degraded to PFCAs, is supported by atmospheric monitoring [7], atmospheric chemistry [8], and global atmospheric modeling studies [9]. Volatilization of PFCAs from sea salt aerosol followed by atmospheric transport has been proposed [10]. The relative importance of the oceanic and atmospheric routes is unclear but is likely to depend on the location, PFCA, and time period under consideration.

Perfluorinated aldehydes, $C_xF_{2x+1}CHO$, are formed during the atmospheric oxidation of HFCs (hydrofluorocarbons), HCFCs (hydrochlorofluorocarbons), and fluorinated alcohols [11,12]. Perfluorinated aldehydes add water to give hydrates which can react with OH radicals to give perfluorocarboxylic acids [13]. The atmospheric oxidation of fluorinated organic compounds into $C_xF_{2x+1}CHO$ followed by hydration and reaction with OH radicals offers a potentially efficient pathway to the formation of perfluorocarboxylic acids which merits further investigation [13]. As part of an effort to improve our understanding of the atmospheric chemistry of perfluorinated aldehyde hydrates (n-$C_xF_{2x+1}CH(OH)_2$), we have used quantum chemical calculations to investigate the structure of n-$C_xF_{2x+1}CH(OH)_2$ and support the assignment of IR spectra. Results are reported herein.

2. Results and discussion

2.1. Structures and equilibrium abundance ratios of $C_xF_{2x+1}CH(OH)_2$ (x = 1–4) isomers

There are six conceivable conformational isomers of $CF_3CH(OH)_2$ based on the orientation of the two OH groups. We classify these isomers by the two dihedral angles of H–C–O–H as follows: AA (180°, 180°), G_+A (60°, 180°), G_-A (−60°, 180°), G_+G_+ (60°, 60°), G_+G_- (60°, −60°), G_-G_+ (−60°, 60°). The structures of these isomers are shown in Fig. 1. The counter parts of optical isomers, e.g. G_-G_- for G_+G_+, AG_- for G_+A and AG_+ for G_-A, are omitted. The normal mode analysis revealed that the G_+G_- and

* Corresponding author. Tel.: +81 3 5841 2119; fax: +81 3 5841 2119.
** Corresponding author.
E-mail addresses: tonokura@esc.u-tokyo.ac.jp (K. Tonokura), twalling@ford.com (T.J. Wallington).
[1] Present address: Department of Micro-Nano Systems Engineering, Nagoya University, Furo-cho, Chikusa-ku, Nagoya 464-8603, Japan.

0022-1139/$ – see front matter © 2008 Elsevier B.V. All rights reserved.
doi:10.1016/j.jfluchem.2008.09.006

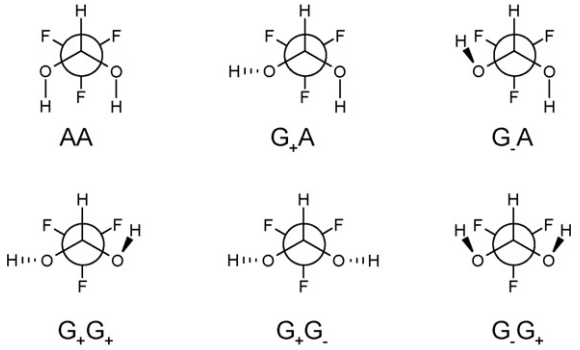

Fig. 1. Conceivable structures of $CF_3CH(OH)_2$ isomers.

G_G+ isomers were found not to be stationary points due to their imaginary mode, thus these structures are not considered further. The relative heats of formation at 0 K (ΔE_0), Gibbs energies at 298 K (ΔG_{298}) and the abundance ratios for the four other isomers predicted by G3//B3LYP and G3(MP2)//B3LYP calculations are listed in Table 1. In the calculation of ΔG_{298} and the abundance ratios, we take the number of optical isomers into account. As shown in Fig. 2a, the most stable structure of $CF_3CH(OH)_2$ is G_A, which has one intramolecular hydrogen bond between F and H atoms with a distance of 2.38 Å. The abundance ratio of the G+A isomer to the G_A isomer was estimated to be 0.15 at G3//B3LYP level of theory, indicating that the G+A isomer must be taken into account at ambient temperature.

Although an experimental IR absorption spectrum is not available, we calculated structures and absorption spectra of the $C_2F_5CH(OH)_2$ isomers. The additional dihedral angle in $C_2F_5CH(OH)_2$ leads to 12 conceivable isomers denoted as A-AA, A-G+A, A-G_A, A-G+G+, A-G+G_, A-G_G+, G-AA, G-G+A, G-G_A, G-G+G+, G-G+G_ and G-G_G+, where the first A/G denotes the dihedral angle of the carbon skeleton and optical isomers are omitted. Similar to $CF_3CH(OH)_2$, the two C_s symmetric isomers A-G+G_ and A-G_G+ had an imaginary vibrational mode indicating that these structures are transition structures. Moreover, the two optimized structure with C_1 symmetry, G-G+G_ and G-G_G+, could not be

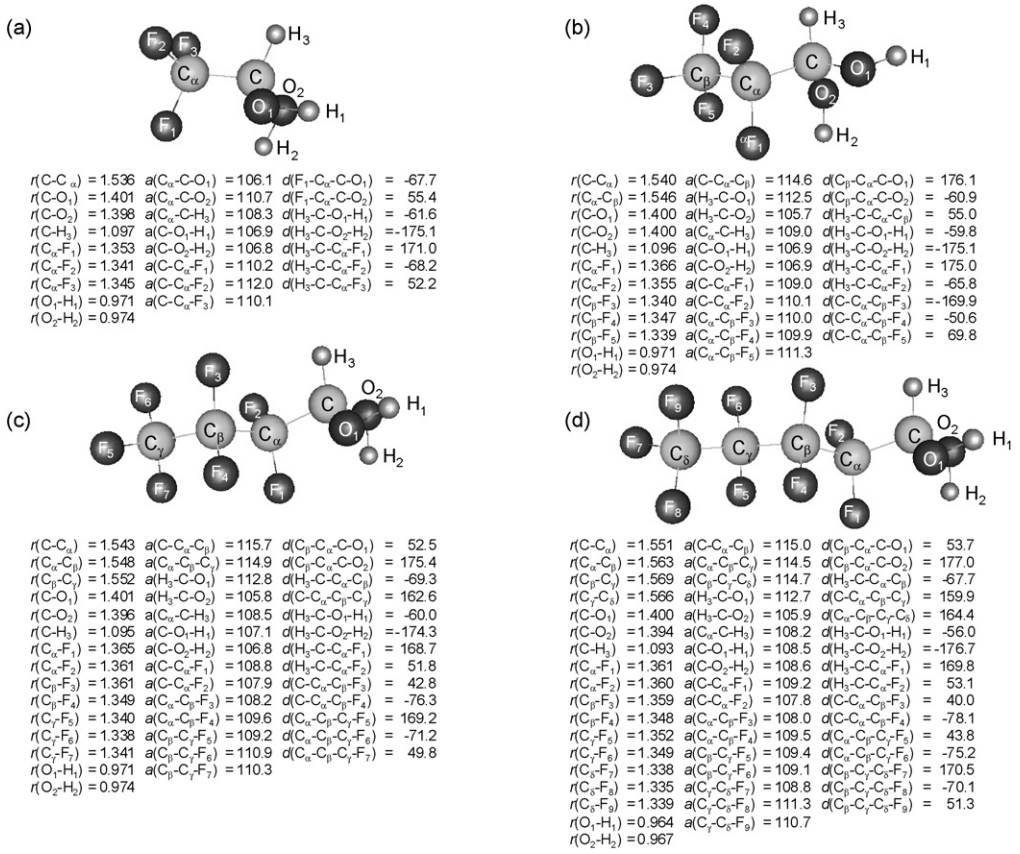

Fig. 2. Geometries of the most stable isomers of $C_xF_{2x+1}CH(OH)_2$ (x = 1 (a), 2 (b), and 3 (c)) optimized at B3LYP/6-31G(d) level of theory, and $C_4F_9CH(OH)_2$ (d) optimized at B3LYP/6-311+G(d,p) level of theory. In all figures, distances are in units of Å and angles are in units of degrees.

Table 1
Relative heats of formation at 0 K (ΔE_0), Gibbs energies at 298 K (ΔG_{298}) and abundance ratios of $CF_3CH(OH)_2$ isomers.

Isomer		ΔE_0 (kJ mol^{-1})		ΔG_{298} (kJ mol^{-1})		Abundance ratio @ 298 K	
		G3//B3LYP	G3(MP2)//B3LYP	G3//B3LYP	G3(MP2)//B3LYP	G3//B3LYP	G3(MP2)//B3LYP
G_A	C_1	0.00	0.00	0.00	0.00	1.00	1.00
G+A	C_1	4.66	4.48	4.71	4.54	0.15	0.16
AA	C_s	5.36	5.24	6.74	6.62	0.07	0.07
G+G+	C_1	9.54	9.40	8.71	8.57	0.03	0.03

Table 2
Relative heats of formation at 0 K (ΔE_0), Gibbs energies at 298 K (ΔG_{298}) and abundance ratios of n-$C_2F_5CH(OH)_2$ isomers calculated at G3(MP2)//B3LYP level of theory.

Isomer		ΔE_0 (kJ mol^{-1})	ΔG_{298} (kJ mol^{-1})	Abundance ratio @ 298 K
G-G_A	C_1	0.00	0.00	1.00
A-G_A	C_1	1.52	2.37	0.38
G-G$_+$A	C_1	2.75	2.53	0.36
G-AA	C_1	3.05	2.94	0.31
G-G$_+$G$_+$	C_1	6.89	6.17	0.08
A-G$_+$A	C_1	7.13	7.79	0.04
A-G$_+$G$_+$	C_1	9.11	8.16	0.04
A-AA	C_s	10.81	12.12	0.01

found in the present DFT calculations. Table 2 shows the energies and the abundance ratios at 298 K for the other eight isomers predicted by G3(MP2)//B3LYP calculations. As shown in Fig. 2b, the structure of the most stable isomer was found to be G-G_A, which has a hydrogen bond (2.40 Å) connecting a fluorine atom of the CF_2 group to a hydrogen in one of the OH groups. As indicated in Table 2, based upon their relative energies, it is expected that, in addition to the most stable G-G_A isomer, the A-G_A, G-G$_+$A, and G-AA conformations will contribute significantly to the thermal distribution at ambient temperature.

The two dihedral angles in the carbon skeleton of $C_3F_7CH(OH)_2$ lead to 42 conceivable structures (excluding optical isomers). Fig. 3 shows the notations used to describe the dihedral angles of the carbon skeleton used in the following discussion. As with $CF_3CH(OH)_2$ and $C_2F_5CH(OH)_2$, the G_G$_+$ OH structures were found to be transition structures. In the case of the G$_+$G_ OH structures, only the AG$_+$-G$_+$G_ isomer was found to be stable but this conformer is not important under ambient conditions because of its high energy (22.51 kJ mol^{-1} above the most stable [AG$_+$-AG$_+$] conformation). Table 3 summarizes the calculated energies and equilibrium constants at 298 K for all conceivable structures predicted by G3(MP2)//B3LYP calculations. As shown in Fig. 2c, the most stable isomer was found to be the AG$_+$-AG$_+$ structure, which has one hydrogen bond connecting a fluorine atom of the C_α atom with a hydrogen atom in one of the OH groups with a distance of 2.31 Å. The calculated equilibrium constants at 298 K (see Table 3) show that the G$_+$G_-G_A and AG$_+$-G_A isomers make an important contribution under ambient conditions.

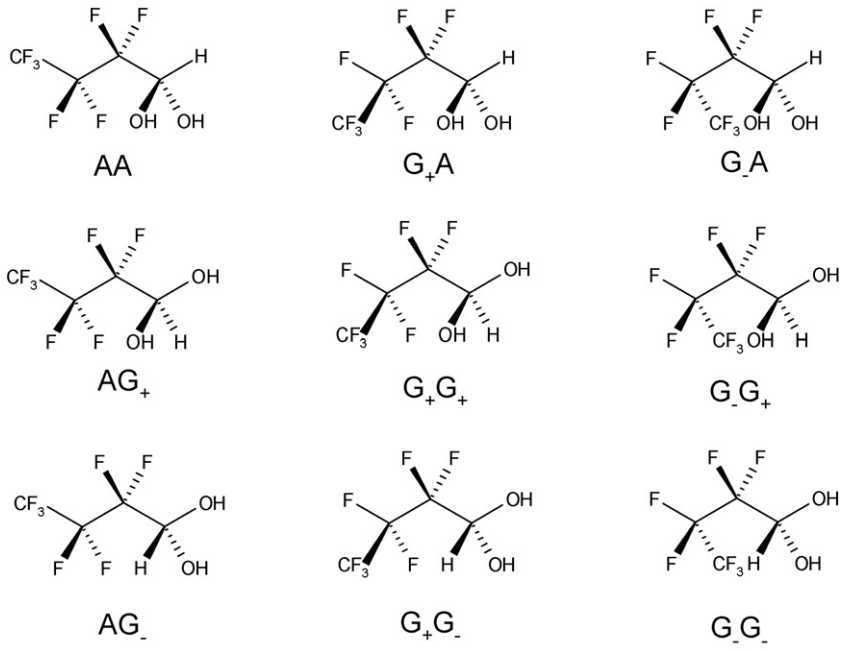

Fig. 3. Notations used to describe the carbon skeleton structure of $C_3F_7CH(OH)_2$ isomers.

Table 3
Relative heats of formation at 0 K (ΔE_0, units of kJ mol^{-1}), Gibbs energies at 298 K (ΔG_{298}, italics, units of kJ mol^{-1}), and abundance ratios (in parentheses) of n-$C_3F_7CH(OH)_2$ isomers calculated at G3(MP2)//B3LYP level of theory.

OH orientation	Carbon skeleton dihedral angles				
	AA	AG$_+$	G$_+$A	G$_+$G$_+$	G$_+$G_
G$_+$G$_+$	14.19, *13.51* (<0.01)	11.01, *9.84* (0.02)	12.85, *14.21* (<0.01)	13.79, *12.91* (0.01)	21.85, *20.85* (<0.01)
AG_	See AA-G$_+$A[a]	10.74, *9.62* (0.02)	14.04, *14.88* (<0.01)	Unstable	9.43, *7.81* (0.04)
AG$_+$	See AA-G_A[a]	0.00, *0.00* (1.00)	10.82, *12.15* (0.01)	6.230, *5.95* (0.09)	6.45, *5.56* (0.11)
AA	16.04, *22.08* (<0.01)	6.33, *6.06* (0.09)	17.89, *17.87* (<0.01)	15.47, *15.69* (<0.01)	8.56, *7.73* (0.04)
G_A	5.04, *5.87* (0.09)	3.74, *3.40* (0.25)	9.41, *10.24* (0.02)	6.88, *7.97* (0.04)	2.66, *2.36* (0.39)
G$_+$A	10.42, *10.57* (0.01)	6.87, *6.06* (0.09)	12.23, *14.26* (<0.01)	7.84, *8.50* (0.03)	13.27, *12.58* (0.01)
G_G_	See AA-G$_+$G$_+$[a]	–[b]	13.49, *12.87* (0.01)	–[b]	13.06, *11.53* (0.01)
G$_+$G_	–[b]	22.51, *20.84* (<0.01)	–[b]	–[b]	–[b]
G_G$_+$	–[b]	–[b]	–[b]	–[b]	–[b]

[a] Optical isomers.
[b] Optimized structures were not found in the present study.

The three dihedral angles in the carbon skeleton of *n*-$C_4F_9CH(OH)_2$ lead to 123 conceivable structures excluding optical isomers. In the present study, only the most stable isomer by analogy to the smaller hydrates (AAG_+-AG_+) was calculated. As shown in Fig. 2d, the AAG_+-AG_+ isomer has one hydrogen bond connecting a fluorine atom of the C_α atom to a hydrogen atom in one of the OH groups with a distance of 2.39 Å at B3LYP/6-311+G(d, p) level of theory.

2.2. Assignment of IR spectra of *n*-$C_xF_{2x+1}CH(OH)_2$ (*x* = 1–4)

Figs. 4a, 6a, and 7a show the IR spectra of $C_xF_{2x+1}CH(OH)_2$ (*x* = 1, 3, 4) measured in 700 Torr of air diluent at 296 K using a spectral resolution of 0.25 cm^{-1} in the smog chamber facility at Ford Motor Company [13]. To simulate the IR spectra of *n*-$C_xF_{2x+1}CH(OH)_2$ (*x* = 1–4), we performed a normal mode analysis at B3LYP/6-311+G(d,p) level of theory with the wavenumber-linear scaling (WLS) method [14] for the optimized structures described above. For comparison between experimental and calculated results, we assumed the Lorenz type line shape with a full width at half maximum of 20 cm^{-1}. Fig. 4 shows IR spectra of $CF_3CH(OH)_2$. The calculated composite spectrum of the equilibrium mixture of conformers at ambient temperature shown in Fig. 4b is in good agreement with the experimental spectrum of $CF_3CH(OH)_2$ shown in Fig. 4a. In the experimental spectrum there were two OH stretching modes around 3600 cm^{-1}. In the calculated spectra of the G_A and G_+A isomers, these two modes were separated by 43 and 26 cm^{-1} after WLS correction and are assigned to the OH groups with (low frequency mode) and without (high frequency mode) hydrogen bonding. In the case of the AA and G_+G_+ isomers, the symmetric and antisymmetric stretching modes of the two OH groups have a similar frequency resulting in the single feature at approximately 3600 cm^{-1} in Fig. 4e and f.

Fig. 5b–e shows the calculated absorption spectra of the G-G_A, A-G_A, G-G_+A and G-AA isomers of *n*-$C_2F_5CH(OH)_2$. As with $CF_3CH(OH)_2$, two OH stretching modes of the G-G_A, A-G_A and G-G_+A isomers were assigned to OH groups with (low frequency), and without (high frequency), hydrogen bonding. As indicated in Fig. 5e, the symmetric and antisymmetric modes associated with the OH groups in the G-AA isomer have a similar frequency.

Fig. 6 shows experimental (a) and calculated (b–f) absorption spectra of *n*-$C_3F_7CH(OH)_2$. The composite thermal average spectrum shown in Fig. 6b of the four lowest energy isomers (AG_+-AG_+(6c), G_+G_--G_A(6d) AG_+-G_A(6e) and G_+G_--AG_+(6f)) is in excellent agreement with the experimentally measured spectrum (a). Each of the four isomers shown in Fig. 6 has two O–H stretching modes associated with OH groups with and without hydrogen bonding. In the experimental spectrum (a) there are two absorption bands in the range 900–1000 cm^{-1}. In contrast, the calculated spectra for each isomer (c–f) only have a single band in the 900–1000 cm^{-1} region, assigned to the in-phase stretching mode of (CF_3)–$(C_2F_4CH(OH)_2)$ and (C_3F_7)–$(CH(OH)_2)$ bonds. The frequency of this stretching mode depends on the carbon skeleton structure of the isomer and is 896.6, 892.5, 949.6 and 945.0 cm^{-1} (after WLS correction) for the AG_+-AG_+, AG_+-G_A, G_+G_--G_A and G_+G_--AG_+ isomers, respectively. The composite thermal average spectrum of the four isomers (b) has two absorption bands in the 900–1000 cm^{-1} region in good agreement with the experimental result (a).

Fig. 7 shows experimental (a) and calculated (b) absorption spectra of *n*-$C_4F_9CH(OH)_2$. Again, two O–H stretching modes are evident and are associated with OH groups with, and without, hydrogen bonding. Similar to the discussion above for

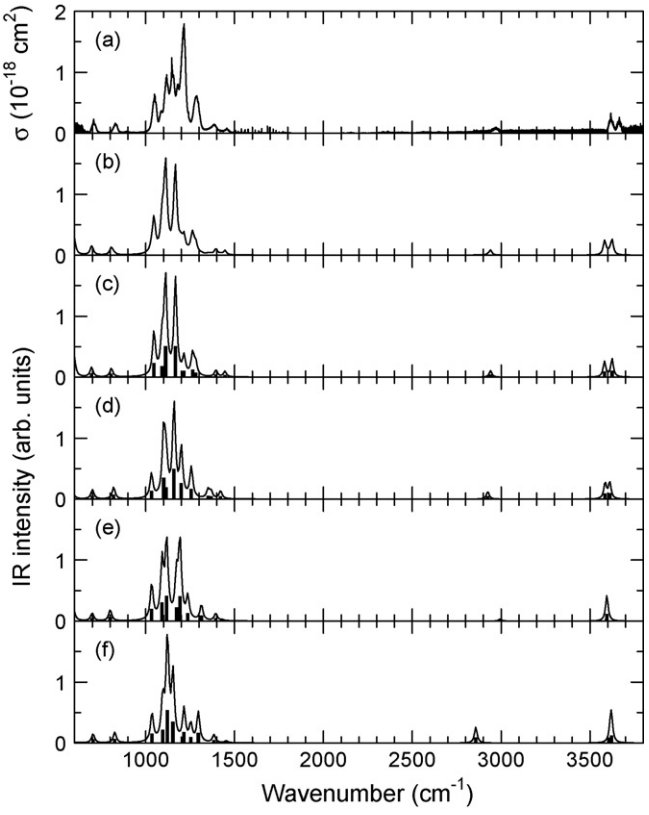

Fig. 4. IR absorption spectra of $CF_3CH(OH)_2$ isomers: (a) experimental results; (b) thermal average of calculated isomers; (c) G_A; (d) G_+A; (e) AA; (f) G_+G_+. The bars in panels (c)–(f) are the integrated absorption cross-sections predicted by the quantum chemical calculations, the lines are absorption spectra calculated assuming each peak is described by a Lorenz function with a full width at half maximum of 20 cm^{-1}.

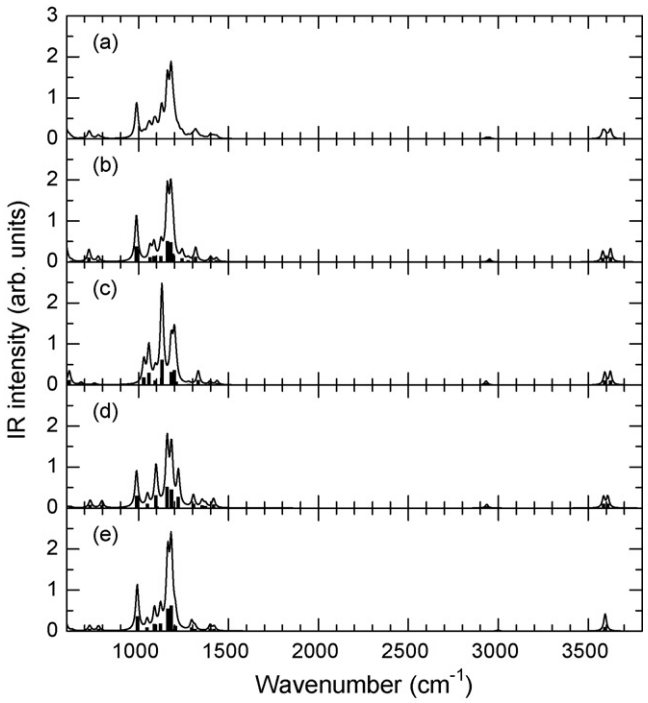

Fig. 5. IR absorption spectra of $C_2F_5CH(OH)_2$ isomers: (a) thermal average of calculated isomers; (b) G-G_A; (c) A-G_A; (d) G-G_+A; (e) G-AA. The bars are integrated absorption cross-section predicted by quantum chemical calculations, the lines are absorption spectra calculated assuming that each peak is described by a Lorenz function with a full width at half maximum of 20 cm^{-1}.

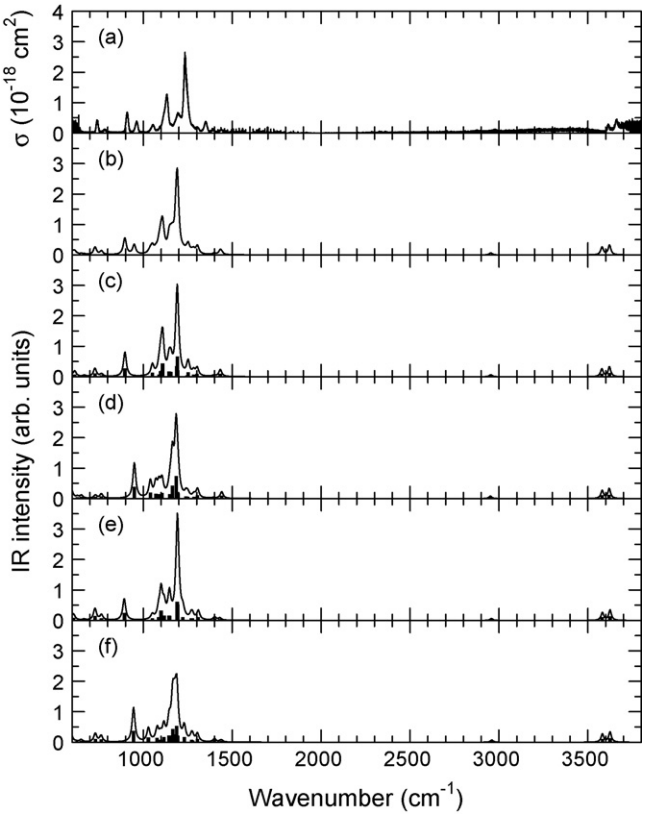

Fig. 6. IR absorption spectra of $C_3F_7CH(OH)_2$ isomers: (a) experimental results; (b) thermal average of calculated isomers; (c) AG_+-AG_+; (d) G_+G_--G_-A; (e) AG_+-G_-A; (f) G_+G_--AG_+. The bars in panels (c)–(f) are integrated absorption cross-sections predicted by quantum chemical calculations, the lines are absorption spectra calculated assuming that each peak is described by a Lorenz function with a full width at half maximum of 20 cm^{-1}.

n-$C_3F_7CH(OH)_2$, there are two absorption bands in the 800–900 cm^{-1} region in the experimental spectrum, whereas only a single band in the calculated spectrum, suggesting contributions from isomers with different carbon skeleton structures.

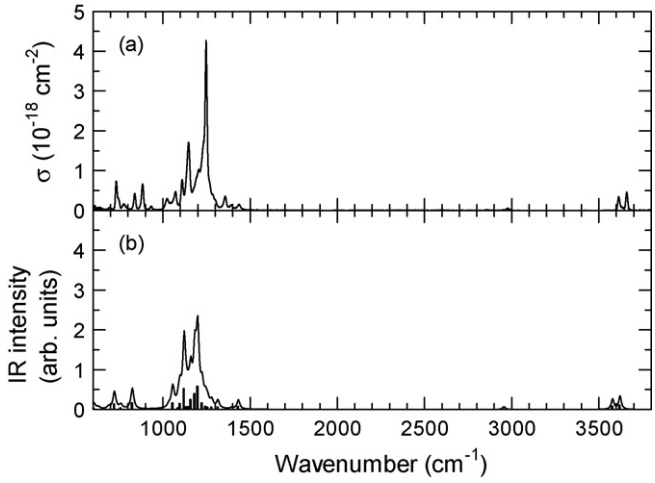

Fig. 7. IR absorption spectra of $C_4F_9CH(OH)_2$ obtained from experiments (a) and calculated for the isomer with AAG_+-AG_+ geometry (b). The bars in panel (b) are integrated absorption cross-sections predicted by quantum chemical calculations, the line is the absorption spectrum calculated assuming that each peak is described by a Lorenz function with a full width at half maximum of 20 cm^{-1}.

3. Conclusions

Quantum chemical calculations have been performed to determine the molecular structure and IR spectra of *n*-$C_xF_{2x+1}CH(OH)_2$ (x = 1–4). We show that intramolecular hydrogen bonding is present in the lowest energy conformers of *n*-$C_xF_{2x+1}CH(OH)_2$ (x = 1–4). Weak intramolecular hydrogen bonding has also been reported for the structurally similar fluorotelomer alcohols *n*-$C_xF_{2x+1}CH_2CH_2OH$ [15]. Experimental spectra of the hydrates *n*-$C_xF_{2x+1}CH(OH)_2$ (x = 1, 3, 4) are well described by composite spectra constructed from the calculated spectra for different conformational isomers weighted according to their predicted abundance at 298 K. Under ambient conditions the hydrates *n*-$C_xF_{2x+1}CH(OH)_2$ (x = 1–4) exist as mixtures of their conformational isomers. Distinct features attributable to the different isomers are visible in the experimental spectra measured at 296 K. The hydrates *n*-$C_xF_{2x+1}CH(OH)_2$ are removed from the atmosphere by reaction with OH radicals and by wet and/or dry deposition [13]. Reaction with OH radicals occurs via hydrogen atom abstraction and involves breaking the C–H bond. The chemical environment of the C–H bond in the different conformers is very similar and we would expect that the atmospheric chemistry of the conformers is, for all practical purposes, indistinguishable.

4. Computational methods

Quantum chemical calculations were carried out using the Gaussian 03 series of programs [16]. The geometry optimization and frequency calculations of perfluorinated aldehyde hydrates were performed by density functional theory with the B3LYP functional using the standard Gaussian 6-31G(d) and 6-311+G(d,p) basis sets. The B3LYP uses Beck's gradient corrected exchange functional [17], Lee-Yang-Parr's gradient corrected correlation functional, and Beck's three parameter hybrid HF/DFT method [18] using Lee-Yang-Parr's correlational functional. The structures of all conceivable isomers of *n*-$C_xF_{2x+1}CH(OH)_2$ (x = 1–3) were optimized. In the case of *n*-$C_4F_9CH(OH)_2$, only the most stable isomer (chosen by analogy to the most stable isomer for x = 1–3) was optimized. For $CF_3CH(OH)_2$ isomers, Gaussian-3 (G3)//B3LYP, and its variation G3(MP2)//B3LYP, calculations [19] were performed to obtain energies and equilibrium constants, whereas only G3(MP2)//B3LYP calculations were carried out for $C_2F_5CH(OH)_2$ and $C_3F_7CH(OH)_2$ isomers. In the G3//B3LYP and G3(MP2)//B3LYP methods, the initial geometries and zero-point energies are obtained from B3LYP density functional theory [B3LYP/6-31G(d)]. The IR absorption spectra of calculated hydrates were predicted by the B3LYP/6-311+G(d,p) level of theory using the wavenumber-linear scaling (WLS) method [14].

Acknowledgements

The authors thank H. Chishima for earlier stage of calculations. KT thanks The Japan Securities Scholarship Foundation for a research grant.

Appendix A. Supplementary data

Supplementary data associated with this article can be found, in the online version, at doi:10.1016/j.jfluchem.2008.09.006.

References

[1] C.A. Moody, J.W. Martin, W.C. Kwan, D.C.G. Muir, S.A. Mabury, Environ. Sci. Technol. 36 (2002) 545–551.
[2] C.A. Moody, W.C. Kwan, J.W. Martin, D.C.G. Muir, S.A. Mabury, Anal. Chem. 73 (2001) 2200–2206.

[3] J.W. Martin, M.M. Smithwick, B.M. Braune, P.F. Hekstra, D.C.G. Muir, S.A. Mabury, Environ. Sci. Technol. 38 (2004) 373–380.
[4] Determination of low levels of fluoropolymer polymerization aids—a guidance document, The Society of the Plastics Industry, SPI Literature Catalogue # BZ-102, New York, 2003.
[5] D.A. Ellis, S.A. Mabury, J.W. Martin, D.C.G. Muir, Nature 412 (2001) 321–324.
[6] K. Prevedouros, I.T. Cousins, R.C. Buck, S.H. Korzeniowski, Environ. Sci. Technol. 40 (2006) 32–44.
[7] M. Shoeib, T. Harner, P. Vlahos, Environ. Sci. Technol. 40 (2006) 7577–7583.
[8] D.A. Ellis, J.W. Martin, A.O. De Silva, S.A. Mabury, M.D. Hurley, M.P. Sulbaek Andersen, T.J. Wallington, Environ. Sci. Technol. 38 (2004) 3316–3321.
[9] T.J. Wallington, M.D. Hurley, J. Xia, D.J. Wuebbles, S. Sillman, A. Ito, J.E. Penner, D.A. Ellis, J.W. Martin, S.A. Mabury, C.J. Nielsen, M.P. Sulbaek Andersen, Environ. Sci. Technol. 40 (2006) 924–930.
[10] C.J. McMurdo, D.A. Ellis, E. Webster, J. Butler, R.D. Christensen, L.K. Reid, Environ. Sci. Technol. 42 (2008) 3969–3974.
[11] M.D. Hurley, J.C. Ball, T.J. Wallington, M.P. Sulbaek Andersen, D.A. Ellis, J.W. Martin, S.A. Mabury, J. Phys. Chem. A 108 (2004) 5635–5642.
[12] M.D. Hurley, T.J. Wallington, M.P. Sulbaek Andersen, D.A. Ellis, J.W. Martin, S.A. Mabury, J. Phys. Chem. A 108 (2004) 1964–1972.
[13] M.P. Sulbaek Andersen, A. Toft, O.J. Nielsen, M.D. Hurley, T.J. Wallington, H. Chishima, K. Tonokura, S.A. Mabury, J.W. Martin, D.A. Ellis, J. Phys. Chem. A 110 (2006) 9854–9860.
[14] H. Yoshida, K. Takeda, J. Okamura, A. Ehara, H. Matsuura, J. Phys. Chem. A 106 (2002) 3580–3586.
[15] R.L. Waterland, M.D. Hurley, J.A. Misner, T.J. Wallington, S.M.L. Melo, K. Strong, R. Dumoulin, L. Castera, N.L. Stock, S.A. Mabury, J. Fluorine Chem. 126 (2005) 1288–1296.
[16] M.J. Frisch, G.W. Trucks, H.B. Schlegel, G.E. Scuseria, M.A. Robb, J.R. Cheeseman, J.A. Montgomery Jr., T. Vreven, K.N. Kudin, J.C. Burant, J.M. Millam, S.S. Iyengar, J. Tomasi, V. Barone, B. Mennucci, M. Cossi, G. Scalmani, N. Rega, G.A. Petersson, H. Nakatsuji, M. Hada, M. Ehara, K. Toyota, R. Fukuda, J. Hasegawa, M. Ishida, T. Nakajima, Y. Honda, O. Kitao, H. Nakai, M. Klene, X. Li, J.E. Knox, H.P. Hratchian, J.B. Cross, C. Adamo, J. Jaramillo, R. Gomperts, R.E. Stratmann, O. Yazyev, A.J. Austin, R. Cammi, C. Pomelli, J.W. Ochterski, P.Y. Ayala, K. Morokuma, G.A. Voth, P. Salvador, J.J. Dannenberg, V.G. Zakrzewski, S. Dapprich, A.D. Daniels, M.C. Strain, O. Farkas, D.K. Malick, A.D. Rabuck, K. Raghavachari, J.B. Foresman, J.V. Ortiz, Q. Cui, A.G. Baboul, S. Clifford, J. Cioslowski, B.B. Stefanov, G. Liu, A. Liashenko, P. Piskorz, I. Komaromi, R.L. Martin, D.J. Fox, T. Keith, M.A. Al-Laham, C.Y. Peng, A. Nanayakkara, M. Challacombe, P.M.W. Gill, B. Johnson, W. Chen, M.W. Wong, C. Gonzalez, J.A. Pople, Gaussian 03, Revision B. 04, Gaussian, Inc., Pittsburgh, PA, 2003 .
[17] A.D. Becke, J. Chem. Phys. 98 (1993) 5648–5652.
[18] C. Lee, W. Yang, R.G. Parr, Phys. Rev. B37 (1988) 785–789.
[19] A.G. Gaboul, L.A. Curtiss, P.C. Redfern, V. Rassolv, J. Chem. Phys. 110 (1999) 7650–7657.